Observation of low-lying electronic states of NiD with multi-isotope analysis

Mahdi Abbasi, Alireza Shayesteh, Patrick Crozet, Amanda Ross

Observation of low-lying electronic states of NiD with multi-isotope analysis

Mahdi Abbasi[1], Alireza Shayesteh[1], Patrick Crozet[2], Amanda J. Ross[2]

[1]School of Chemistry, University of Tehran, I. R. Iran; ashayesteh@ut.ac.ir

[2]Institut Lumière Matière (ILM), Université Lyon1 & CNRS, France; amanda.ross@univ-lyon1.fr

Abstract.

Resolved laser induced fluorescence spectra of ^{58}NiD, recorded at Doppler resolution between 11000 and 18000 cm^{-1} have established more than 200 term energies in two of the three strongly interacting, low-lying states ($^2\Delta$, $^2\Pi$, $^2\Sigma^+$) of NiD, associated with an $Ni^+(3d^9)D^-$ configuration. Our observations span v= 0-5 in the lowest spin-orbit component of the ground state, X $^2\Delta_{5/2}$, v = 0-3 in X $^2\Delta_{3/2}$ and v = 0-1 in the lower component of the W $^2\Pi_{3/2}$ state. Collisional processes populate several neighbouring excited states, allowing us also to locate the first rotational levels of A(Ω = 5/2) v = 1, I(Ω = 3/2) v = 0 and E(Ω = 3/2) v = 1 at 16664.8, 17367.3 and 17508.1 cm^{-1} respectively. Spin-orbit and rotation-electronic interactions are strong in NiD (as in NiH), and with no direct observation of either of the Ω" =1/2 states, meaningful representations of the low-lying energy levels is difficult. We have therefore attempted a global, multi-isotope fit to reproduce the term energies of the known term energies of NiD and ^{58,60,62}NiH (where some Ω" =1/2 levels are known). Dunham-type parameters have been used to represent the unperturbed $^2\Delta$, $^2\Pi$ and $^2\Sigma^+$ states, with off-diagonal matrix elements (treating spin-orbit, *L*- and *S*-uncoupling effects) based on Ni^+ atomic properties. Born-Oppenheimer breakdown terms were included in the model. The equilibrium bond lengths for ^{58}NiH/^{58}NiD are 1.4545(1)/1.4559(1) Å for the X $^2\Delta$ state and 1.5094(2)/1.5083(2) Å for the W $^2\Pi$ state.

Keywords

Laser-induced fluorescence; NiH; NiD; multi-isotope fit; spin-orbit perturbations, Supermultiplet Hamiltonian.

I INTRODUCTION

One of the main motivations for high-resolution spectroscopic investigations of diatomic radicals such as NiD or NiH is to provide benchmark measurements for species whose electronic structure is challenging, but computationally tractable. In their review of transition metal species [1] Langhoff and Bauschlicher underlined the incentive to "develop methods capable not only of accurately describing small systems, but also for modeling larger systems". They illustrated this notion with the Ni atom, because of the problems posed by its near-degenerate low-lying states. Spectroscopy and quantum chemistry have advanced together, striving to understand and reproduce the effects of electron correlation in the bonds formed by transition metals, particularly in a context of materials of catalytic interest. Diatomic molecules such as NiH are the smallest building blocks of such systems. High level *ab initio* methods have become increasingly successful in reproducing molecular energy levels determined from gas-phase spectroscopy as basis set sizes (and computational resources) have grown [2-11]; the calculations on NiH by Marian [11,12], and by Zou and Liu [13], have proven particularly valuable in guiding assignments in our fluorescence spectra. Experimental determinations of the permanent electric dipole moment the B $^2\Delta_{5/2}$ and *X* $^2\Delta_{5/2}$ states in NiH [14], have also provided stringent tests for theory [15-17]. NiH was chosen (Mayhall, ref. [5]) to highlight issues arising in coupled cluster calculations; it has also been used as a benchmark to test the performance of different density functionals, [18,19] with a view to implementing less costly calculations allowing progression from diatomics to larger species. Reliable reference data are therefore important, and gas-phase spectroscopy, in its various forms, provides essential elements for quality control. In this context, we have studied some vibrationally excited levels of the three lowest-lying electronic states ($^2\Sigma^+$, $^2\Pi$ and $^2\Delta$) of NiD.

Electronic transitions in NiH and NiD, formed in flames, vacuum furnace or in hollow cathode discharges, were first studied by photographic techniques [20-23]. The early work was

reviewed by Scullman and co-workers in 1982, who photographed emission spectra of NiH [24] and NiD [25] to resolve some earlier discrepancies, and mapped out the pattern of vibrational levels in some $^2\Delta$ and $^2\Phi$ electronic states. Laser spectroscopy became increasingly important in the1980's. The Field group at MIT – often in collaboration with the Stockholm group – pursued investigations of the electronic states of NiH and NiD with a variety of laser excitation and fluorescence techniques [26,27], observing the W $^2\Pi$ and V $^2\Sigma^+$ low-lying electronic states of NiH in dispersed fluorescence and depletion spectroscopy, and charting excited-state levels on NiH and NiD with $1.5 \leq \Omega' \leq 3.5$, in the energy region 15500 - 19000 cm^{-1}. In parallel, Brown and Urban and their collaborators studied the microwave and infrared transitions within the X $^2\Delta$ ground electronic state of NiH/D using laser magnetic resonance (LMR) techniques [28-32]; these measurements remain the best available to describe the parity splittings in the lowest electronic states of NiD and NiH. Line-lists and combination differences from the electronic spectra reported in the 1980's and early 1990s enabled us to assign many of the bands in our resolved fluorescence spectra of NiD.

The unusual energy level patterns in NiH (and NiD) are the consequence of strong spin-orbit interactions between close-lying electronic states. Zeeman spectra, extensively studied by the Field group [27,33-35], and later in Lyon [36], offer considerable insight into this mixing for the lower electronic states associated with ground state Ni^+ ion, confirming that Λ and Σ become ill-defined quantum numbers as molecular rotation increases. The so-called supermultiplet model, proposed by Gray *et al.* [26,37] and adopted by Marian in her theoretical work [11], was remarkably successful in explaining both the energy level structures and the rotational dependence of g_J Landé factors in $v \leq 2$ vibrational levels of the lowest $^2\Sigma^+$, $^2\Pi$ and $^2\Delta$ states of NiH. It gave a physically meaningful model for the electronic structure of the $Ni^+(3d^9)$ H^- states by taking atomic orbital and spin angular momenta **L** and **S** of the Ni^+ (^2D, d^9) to generate the off-diagonal matrix elements of a molecular

Hamiltonian, where spin-orbit and rotational **L**- and **S**-uncoupling terms introduce mixing between levels of the $^2\Delta$, $^2\Pi$ and $^2\Sigma^+$ states. The supermultiplet description explained the difficulties encountered in fitting infrared and far-infrared transitions in the $X_1\ ^2\Delta_{5/2}$ and $X_2\ ^2\Delta_{3/2}$ states of NiH and NiD with an effective Hamiltonian. Lipus *et al*. [32] reported that attempts to fit ^{x}NiH or ^{x}NiD (x = 58, 60, 61, 62) data with mass-scaled parameters had given unacceptably large standard deviations, and unphysically large Born-Oppenheimer breakdown corrections for H/D substitution; the authors attributed the limitations of their effective Hamiltonain to the influence of unobserved neighbouring levels.

Our purpose was to map out a larger set of energy levels for the low-lying states of NiD, using Fourier transform spectroscopy to resolve laser-induced fluorescence, and to assess the performance of the supermultiplet model when extended to higher energies, and/or with mixed isotopomer input. The original work by Gray *et al* [37] adjusted the parameters of a 15 × 15 energy matrix to represent ro-vibrational energies up to v=2 in each of the low-lying states of ^{58}NiH, with uncertainties in the input energies varying from 0.05 to 1.5 cm^{-1}. The model incorporated off-diagonal contributions between levels with Δv =0 and 1. Subsequent experimental work on NiH [38,39] has provided an extended set of energy levels for ^{58,60,62}NiH, (up to v=4 for $^2\Delta_{5/2}$) with ~0.01 cm^{-1} uncertainty, covering approximately the same energy range as our current work on NiD. This information provides a more stringent test for an expanded supermultiplet description of the low-lying energy levels. The supermultiplet energy matrix has been expanded (to 40 × 40), and now includes off-diagonal terms with $\Delta v \leq 2$, with some additional empirical parameters intended to compensate effects of more remote levels. This approach is successful for NiH in the region where all the vibronic states are observed. After that, fits converge with difficulty, and return increasingly unphysical values for some of the off-diagonal terms. By restricting the number of free parameters in the model (and accepting a larger root-mean-square error in the fit) we reproduce the ensemble of

low-lying rovibronic energies in NiH and NiD reasonably well, although the Ω = 3/2 levels of NiD contribute significantly to the pool of 'outliers' in a multi-isotope fit. These are expected to be strongly affected by spin-orbit mixing with (unobserved) $^2\Pi_{1/2}$ and $^2\Sigma^+$, whose unperturbed positions are 'best estimate extrapolations' derived from NiH data.

II EXPERIMENT

We produced ^{58}NiD in our DC sputter source [40] running with a 150 mA current between a copper loop anode and Ni cathode, with gas pressure around 1 Torr. The water-cooled cathode was drilled to allow a continuous flow of a commercial gas mixture (5% D_2 in Ar, from AirLiquide) through a vacuum chamber. The discharge products were probed by a cw single-mode ring dye laser operating around 17100 or 18100 cm^{-1} (with R6G or pyrromethene 567 dyes), with the laser beam intersecting the discharge plume about 1 cm below the anode. The dye laser was tuned to some of the stronger transitions (B $^2\Delta_{5/2}\leftarrow$X $^2\Delta_{5/2}$ or F $^2\Phi_{7/2}\leftarrow$X $^2\Delta_{5/2}$) transitions reported by Adakkai Kadavathu *et al*. in 1987. Backwards fluorescence was collected and transferred to a commercial FT spectrometer, passing through a λ > 590 nm filter to minimize laser scatter. The fluorescence was much weaker than had been seen (by eye) in NiH with the same set-up, and Fourier-transform resolved fluorescence spectra revealed that collisional energy transfer processes made a smaller contribution to the total fluorescence signal than in NiH. They nevertheless populate the two levels of the D Ω'=3/2 state (also reported by Adakkai Kadavathu and co-workers) and v = 0 of the E Ω'=3/2 state, from which fluorescence occurs to several levels of the two low-lying Ω" =3/2 states. Collisions following excitation of v=1, B $^2\Delta_{5/2}$ populate a second Ω'=5/2 level, that we assign as v=1 of the A state (weak transitions to v=0 were reported in ref.[25]). Tuning the laser to shorter wavelengths, collisions from v=2, B $^2\Delta_{5/2}$ populate another two Ω'=3/2 levels that we label E Ω'=3/2, v=1 and I Ω'=3/2, v=0, scaling from NiH. Figure 1 maps the observed bands whose term

energies could be referenced to the ground electronic state. The direct fluorescence from B $^2\Delta_{5/2}$ to X $^2\Delta_{3/2}$ was very weak, but important in connecting the energy level stacks. Fluorescence from ^{60}NiD and ^{62}NiD was too weak to collect useable interferograms.

Figure 2 illustrates one of the dispersed fluorescence spectra of ^{58}NiD, recorded at 0.04 cm^{-1} resolution (recording time ~2 hours). The laser excited the blend of Q_{ef}(2.5) and Q_{fe}(2.5)1-0 B-X transitions. Comparison with the spectrum pumped via the same transition in NiH (reproduced beneath) shows that collisions populate a quite different selection of excited states. The NiD spectrum is much weaker than NiH, so higher gain settings were used to record the upper spectrum in Fig. 2. Argon atomic lines were more prominent in the NiD spectrum, and scatter from both the pump laser and the spectrometer's internal HeNe laser had to be reduced with optical filters. The high-pass glass filter placed outside the interferometer to remove dye-laser scatter also attenuates the rotational relaxation in the (1-0) B-X band of NiD. Scatter from the HeNe laser was reduced with a notch filter (NF633, Thorlabs) placed in front of the Si-avalanche detector, inside the spectrometer. Most of the B-X (1-1) band was also rejected by the notch filter. In both spectra, emissions following rotationally unselective electronic energy transfer contribute more to the total fluorescence signal than direct emission from the level populated by the laser.

III Analysis

The direct fluorescence back to vibrational levels 0-5 of the X_1 $^2\Delta_{5/2}$ state, with extensive rotational relaxation, was readily assigned on all the ^{58}NiD spectra. Some of the collisionally-induced bands above 14000 cm^{-1} had already been observed and assigned by Adakkai Kadavathu and co-workers[26], and combination differences could be used to confirm most of the excited state assignments for the bands seen at longer wavelength. Loomis-Wood plots were used to make

rotational assignments in the regions where several bands overlap. Combination differences allowed us to reference nearly all the observed transitions to the lowest level of the $X_1\ ^2\Delta_{5/2}$ state (see Figure 1), in a simple term-value fit (given in supplementary data).

Vibrational intervals were very regular for fluorescence series to the $X_1\ ^2\Delta_{5/2}$ state, but vibrational/electronic assignments were less obvious for the **Ω**" = 3/2 states ($X_2\ ^2\Delta_{3/2}$ and $W_1\ ^2\Pi_{3/2}$) in NiD. Guided by mass-scaling the parameters of a 'supermultiplet' fit for ^{58}NiH, we identified the lower electronic states as depicted in Figure 3. The noteworthy features are the irregular vibrational separations, and unusually large e/f parity splittings in the $v'' > 0$ levels of the $X_2\ ^2\Delta_{3/2}$ state. The parity splittings in $X_2\ ^2\Delta_{3/2}$ are sometimes larger than in the other nearby **Ω**" = 3/2 state, nominally $W_1\ ^2\Pi_{3/2}$. We identified some bands from three previously unreported upper state levels, assigning **Ω**' on the basis of first lines in the branches observed. They are v = 1 of the A(**Ω**=5/2) state (with transitions seen only to $X_1\ ^2\Delta_{5/2}$), v=0 of I (**Ω**=3/2) (P and R branches to $W_1\ ^2\Pi_{3/2}$) and v=1 of E(**Ω**=3/2) (P and R branches to only v=0 of $X_2\ ^2\Delta_{3/2}$). Table 1 lists the effective band constants for these excited levels, obtained by fitting the output from the term energy fit to an empirical formula

$$T_{v,J,\Omega,e/f} = T_v + \sum_{m=1,3} Y_{0,m} \left[J(J+1) - \Omega^2\right]^m \pm \frac{1}{2}\left(q_v\,[J(J+1)]^{\Omega} + q_D\,[J(J+1)]^{2\Omega}\right). \quad (1)$$

Levels with e parity take the positive splitting $q_v[(J(J+1)]^{\Omega}$ + … terms in eq (1) , and f parity levels take the negative one. The same approach for the term energies of $X_1\ ^2\Delta_{5/2}$, $X_2\ ^2\Delta_{3/2}$ and $W_1\ ^2\Pi_{3/2}$ states produces the effective band parameters listed in Table 2, where the vibrational intervals and distortion constants for the $X_2\ ^2\Delta_{3/2}$ state underline the inadequacy of this simplistic model. These band parameters give a convenient representation for the observed bands, but have no predictive powers for higher vibrational levels. The supermultiplet approach should allow empirical parameters to be replaced with more physically meaningful ones, offset by a more complicated Hamiltonian. However, there is a serious impediment to this approach for ^{58}NiD. None of the

spectra we have recorded so far has produced fluorescence allowing the low-lying $\Omega = ½$ states ($^2\Sigma^+$ and $^2\Pi_{1/2}$) to be located with respect to the electronic ground state. An isolated branch (around 14800 cm^{-1}) with no resolved parity-splittings is strongly reminiscent of some $\Delta\Omega=0$ transitions between $\Omega = ½$ states seen in NiH spectra [38], but we have no upper state combination differences to link these lines to the assigned systems. To compensate the gap in information, we opted for a multi-isotope deperturbation analysis, fitting ro-vibrational term values up to 6500 cm^{-1} for the three strongly-interacting low-lying electronic states ($^2\Delta$, $^2\Pi$ and $^2\Sigma^+$) for ^{x}NiH and NiD. ^{58}NiD term energies came from this analysis. Energy level data for ^{x}NiH (x = 58, 60 and 62) were taken from earlier work from the Lyon group [38,39].

IV Supermultiplet Hamiltonian : extension and modification.

The effective parameters of Tables 1 and 2 give a crude but convenient model for recognizing the lines seen in the spectra. Aiming to produce a model with better predictive powers for the lowest electronic states, we proceeded to fit the low-lying energy levels in NiH and NiD in an slightly modified version of the 'supermultiplet' model used by Gray and co-workers [26]. The challenge was to extend this physically reasonable model to higher vibrational levels (we observe up to $v = 5$ in the $X_1\ ^2\Delta_{5/2}$ state of NiD, but fewer levels of the other states, see table 4), and to use appropriate isotopic scaling of parameters (defined for ^{58}NiH) so that they reproduce measured energy levels of other isotopic forms (^{60,62}NiH, ^{58}NiD).

We chose to take Brown's $\boldsymbol{N^2}$-effective Hamiltonian [41-43] for the 'unperturbed' basis states, for which vibrational, rotational, spin-orbit, spin rotation and Λ-doubling parameters were represented by simple Dunham-type parameters, $x_v = x_e + \sum_{k+1} x_k \left(v + \frac{1}{2} \right)^k$. (2)

The $X\ ^2\Delta$, $W\ ^2\Pi$ and $V\ ^2\Sigma^+$ electronic basis states were thus represented by

$$H_{eff} = T_v + G_v + B_v\mathbf{N}^2 - D_v\mathbf{N}^4 + \gamma_v\mathbf{N}.\mathbf{S} + \gamma_{D,v}\mathbf{N}^2\left(\mathbf{N}.\mathbf{S}\right) + A_v\mathbf{L}.\mathbf{S}$$
$$+\frac{1}{2}\left[\left(p_v^{\Pi}+q_v^{\Pi}\right)\left(S_+^2+S_-^2\right)-\left(p_v^{\Pi}+2q_v^{\Pi}\right)\left(J_+S_+ + J_-S_-\right)+q_v^{\Pi}\left(J_+^2+J_-^2\right)-p_v^{\Delta}\left(J_+^3S_+ + J_-^3S_-\right)+q_v^{\Delta}\left(J_+^4+J_-^4\right)\right] \quad (3)$$

The spin-orbit parameter A was assumed to be isotopically invariant. When it could not be determined from experimental data, it was constrained to the free Ni^+ ion value (-603 cm^{-1}). Vibrational dependence could be determined only for the X $^2\Delta$ state in NiH, so simple mass scaling

$A_v^{(\alpha)} = A_e^{(1)}\sqrt{\left(\frac{\mu_{(1)}}{\mu_{(\alpha)}}\right)}\left(v+\frac{1}{2}\right)$ provided an initial value for A_1 in NiD.

We found that the 'supermultiplet' model struggled to reproduce the lowest NiH energy levels to their estimated experimental uncertainty, and interpreted this as the consequence of truncation of the off-diagonal terms at $\Delta v \leq 2$. Introducing empirical spin-rotation (γ) and Λ–doubling (p and q) parameters in eq. (3) compensated these problems in the lowest vibrational levels. As they are accounting only for effects of remote states, these terms were expected to be small. They were assumed to scale isotopically according to their dependences on B_v (given in refs [28, 44]);

$$p_v^{\Pi} = \frac{4\,\zeta_{3d}B_v}{E_{\Pi,v}-E_{\Sigma,v'}} \quad ,$$

$$q_v^{\Pi} = \frac{4\,B_v^{\,2}}{E_{\Pi,v}-E_{\Sigma,v'}} ,$$

$$p_v^{\Delta} = \frac{96\zeta_{3d}B_v^{\,3}}{\left(E_{\Delta,v}-E_{\Sigma,v'}\right)\left(E_{\Delta,v}-E_{\Pi,v'}\right)^2} \quad \text{and}$$

$$q_v^{\Delta} = \frac{48\,B_v^{\,4}}{\left(E_{\Delta,v}-E_{\Sigma,v'}\right)\left(E_{\Delta,v}-E_{\Pi,v'}\right)^2} \quad .$$

Having chosen to work with the $\mathbf{N^2}$ Hamiltonian, we had to incorporate the difference in electronic term energies associated with the $\mathbf{R^2}$ and $\mathbf{N^2}$ Hamiltonians when using ^{58}NiH parameters to calculate energies of isotopically substituted forms. The difference between electronic energy origins for the different $^2\Lambda$ states when expressed in $\mathbf{R^2}$ or $\mathbf{N^2}$ forms is

$$\left\langle {}^{2S+1}\Lambda \left| B(R)\left(\mathbf{R}^2-\mathbf{N}^2\right)\right| {}^{2S+1}\Lambda \right\rangle = B_\Lambda(R)\left[L(L+1)-2\Lambda^2\right] \quad , \qquad (4)$$

where $B_\Lambda(R)$ is rotational constant of the $^2\Lambda$ state, and L = 2 (associated with the Ni^+ $3d^9$ configuration) Setting $T_\Lambda(\mathbf{R}^2) + B_\Lambda\mathbf{R}^2$ equal to $T_\Lambda(\mathbf{N}^2)+ B_\Lambda\mathbf{N}^2$, we obtained the following relations:

$$T_\Delta\left(\mathbf{N}^2\right)-T_\Delta\left(\mathbf{R}^2\right)=-2B_\Delta \qquad (5a)$$

$$T_\Pi\left(\mathbf{N}^2\right)-T_\Pi\left(\mathbf{R}^2\right)=-2B_\Pi \qquad (5b)$$

$$T_\Sigma\left(\mathbf{N}^2\right)-T_\Sigma\left(\mathbf{R}^2\right)=(0.86)^2\times 6B_\Sigma \qquad (5c)$$

T_e for the $^2\Delta$ state is taken to be zero in both $\mathbf{R}^2$ and $\mathbf{N}^2$ models, so the energy shifts for equilibrium term energies T_e of the $^2\Pi$ and $^2\Sigma^+$ states become:

$$T_{e,\Pi}\left(\mathbf{N}^2\right)-T_{e,\Pi}\left(\mathbf{R}^2\right)=4B_{e,\Pi}+2B_{e,\Delta} \qquad (6a)$$

$$T_{e,\Sigma}\left(\mathbf{N}^2\right)-T_{e,\Sigma}\left(\mathbf{R}^2\right)=(0.86)^2\times 6B_{e,\Sigma}+2B_{e,\Delta} \qquad (6b)$$

$T_{v,\Lambda}$ $B_{v,\Lambda}$ etc were calculated for isotopically substituted forms according to Le Roy's formulation[45] from Dunham-type parameters for each state,

$$Y_{l,m}^{(\alpha)}=\left[Y_{l,m}^{(1)}+\frac{\Delta M_H^{(\alpha)}}{M_H^{(\alpha)}}\delta_{l,m}^{H}+\frac{\Delta M_{Ni}^{(\alpha)}}{M_{Ni}^{(\alpha)}}\delta_{l,m}^{Ni}\right]\left(\frac{\mu_1}{\mu_\alpha}\right)^{m+l/2} \qquad (7)$$

where $\delta_{l,m}^{H}$ and $\delta_{l,m}^{Ni}$ are Born-Oppenheimer breakdown correction parameters; $\Delta M_X^{(\alpha)} = M_X^{(\alpha)} - M_X^{(1)}$, $M_H^{(x)}$ and $M_{Ni}^{(x)}$ represent the atomic masses of the *H* and *Ni* atoms, and μ the reduced masses.

Brown and Watson [46] have given analogous reduced-mass scaling relationships for the spin–rotation terms, $\gamma_{l,m}^{(\alpha)} = \gamma_{l,m}^{(1)} \left(\frac{\mu^{(1)}}{\mu^{(\alpha)}} \right)^{1+m+\frac{l}{2}}$.

For the Λ-doubling parameters, we take :

$$p_{l,m}^{(\alpha)}(\Pi) = p_{l,m}^{(1)}(\Pi) \left(\frac{\mu_1}{\mu_\alpha} \right)^{1+m+l/2},$$

$$q_{l,m}^{(\alpha)}(\Pi) = q_{l,m}^{(1)}(\Pi) \left(\frac{\mu_1}{\mu_\alpha} \right)^{2+m+l/2},$$

$$p_{l,m}^{(\alpha)}(\Delta) = p_{l,m}^{(1)}(\Delta) \left(\frac{\mu_1}{\mu_\alpha} \right)^{3+m+l/2} \text{ and}$$

$$q_{l,m}^{(\alpha)}(\Delta) = q_{l,m}^{(1)}(\Delta) \left(\frac{\mu_1}{\mu_\alpha} \right)^{4+m+l/2}$$

Although they were expected to be significant for hydrogen/deuterium substitution, the leading Born-Oppenheimer breakdown parameters δ_{00}^{H} , δ_{10}^{H} could not be determined in a statistical sense from the data available, because they are strongly correlated with vibrational off-diagonal parameters $f_{\Lambda\Lambda'}$. We used eq. (7) to calculate the shifts in energy origins for the $^2\Lambda$ electronic states of NiD relative to those of NiH based on the differences in $\mathbf{R}^2$ and $\mathbf{N}^2$ Hamiltonians (eq. 4), and

then held these (effective) $\delta^H_{0,0}$ parameters fixed in the fit. The resulting expressions, and their numerical values, are :

$$T_{e,\Lambda}\left(NiD\right)-T_{e,\Lambda}\left(NiH\right)=\left(\frac{M^D-M^H}{M^H}\right)\delta^H_{00}\left(\Lambda\right)$$

$$\delta^H_{02}\left(\Delta\right)=-0.9\left(\frac{M^D}{M^D-M^H}\right)\times\left[4B_{e(\Pi)}+2B_{e(\Delta)}\right]\times\left[\left(\frac{\mu_{NiH}}{\mu_{NiD}}\right)-1\right] \approx \text{-45 cm}^{-1}\ ,$$

$$\left\langle {}^2\Delta_{3/2}\left|\hat{\mathbf{H}}_{\text{rot}}+\hat{\mathbf{H}}_{\text{SO}}\right|{}^2\Pi_{3/2}\right\rangle \ = \ -603f_{v_\Delta,v_\Pi}+2B_{v_\Delta,v_\Pi} \ \approx \text{-49 cm}^{-1}.$$

Nickel isotope substitution was treated in the same way, constraining the values $\delta^{Ni}_{00}\left(\Pi\right)=-0.8$ and $\delta^{Ni}_{00}\left(\Sigma\right)=-0.9$ cm^{-1} in the multi-isotope fits. The δ^H_{01} parameters were strongly correlated with the off-diagonal $B_{vv'}$ parameters, and were set to zero. Only one Born-Oppenheimer breakdown parameter was finally optimized in our fits : $\delta^H_{02}\left(\Delta\right)$ = -4.07 (14) × 10^{-5} cm^{-1}, for the $^2\Delta$ state. It gave a small improvement to the overall root-mean-square deviation of the fit by reducing obs-calc deviations for the higher J levels in v=0 of the $^2\Delta$ state of NiD.

Off-diagonal spin-orbit mixing terms have been taken from the $\boldsymbol{R^2}$ supermultiplet model detailed by Gray *et al*. These included spin-orbit coupling terms producing the strong mixing between $^2\Delta_{3/2}$ and $^2\Pi_{3/2}$ states and between $^2\Pi_{1/2}$ and $^2\Sigma^+$ states, originating from $\zeta_{\text{Ni+ }3d}$ (-603 cm^{-1}). The parameters $A_{\Pi\Delta}$ and $A_{\Sigma\Pi}$ are scaled by a vibrational overlap factor, $f_{\Pi\Delta}$ (or $f_{\Sigma\Pi}$), largest for Δv = 0 but nonzero elsewhere. Gray's additional scaling coefficient $c_{\Sigma\Pi}$ of 0.86, justified by indications from *ab initio* work that the low-lying $^2\Sigma^+$ state has around 25% Ni 3d^{10} character, was applied to all $^2\Pi \sim {}^2\Sigma^+$ matrix elements (eqs. 11, 12). The vibrational overlap integrals $f_{v_\Lambda,v_{\Lambda'}}=\left\langle v_{\Lambda,}\left|v_{\Lambda',}\right\rangle\right.$, and rotationally-

dependent terms, $B_{v_\Lambda, v_{\Lambda'}} = \frac{\hbar^2}{2\mu}\left\langle v_{\Lambda,}\left|\frac{1}{r^2}\right|v_{\Lambda',}\right\rangle$, were calculated using Le Roy's program LEVEL[47], taking as input the RKR potentials calculated [48] from Dunham-type representations of G_v and B_v (eq. (2)).

Matrix elements coupling the $^2\Delta$, $^2\Pi$ and $^2\Sigma^+$ states are then:

$$\left\langle {}^2\Delta_{5/2}\left|\hat{\mathbf{H}}_{\rm rot}+\hat{\mathbf{H}}_{\rm SO}\right|{}^2\Pi_{3/2}\right\rangle = -2B_{v_\Delta, v_\Pi}\times\sqrt{\left(J+5/2\right)\left(J-3/2\right)} \quad (8)$$

$$\left\langle {}^2\Delta_{3/2}\left|\hat{\mathbf{H}}_{\rm rot}+\hat{\mathbf{H}}_{\rm SO}\right|{}^2\Pi_{3/2}\right\rangle = -603 f_{v_\Delta, v_\Pi}+2B_{v_\Delta, v_\Pi} \quad (9)$$

$$\Delta E^f_{Spin-rotation} = 0.5\left(\gamma+\gamma_D x\right)\left(N+1\right) \quad (10)$$

$$\left\langle {}^2\Pi_{3/2}\left|\hat{\mathbf{H}}_{\rm rot}+\hat{\mathbf{H}}_{\rm SO}\right|{}^2\Sigma^+_{1/2}\right\rangle = -0.86\times\sqrt{6}B_{v_\Pi, v_\Sigma}\times\sqrt{\left(J-1/2\right)\left(J+3/2\right)} \quad (11)$$

$$\left\langle {}^2\Pi_{1/2}\left|\hat{\mathbf{H}}_{\rm rot}+\hat{\mathbf{H}}_{\rm SO}\right|{}^2\Sigma^+_{1/2}\right\rangle = \frac{1}{2}\left[-603\times 0.86\times\sqrt{6}f_{v_\Pi, v_\Sigma}\right]+0.86\times\sqrt{6}B_{v_\Pi, v_\Sigma}\times\left[1\mp\left(J+1/2\right)\right], \quad (12)$$

where upper/lower sign applies to levels of *e*/*f* parity. The matrix elements are given in Table 4.

The Dunham-type (rounded) parameters returned from the non-linear least-squares fit (subroutine NLLSSRR.f from Le Roy's DParFit program [49]) are listed in Table 5. The vibrational overlap integrals needed in the off-diagonal terms are given in Table 6a, and the off-diagonal rotational terms in Table 6b.

Given the unbalanced data set, with significantly less information on the $^2\Sigma^+$ and $^2\Pi_{1/2}$ states of NiH (and none at all for NiD) than for $^2\Pi_{3/2}$, $^2\Delta_{3/2}$ and $^2\Delta_{5/2}$ states, it was not particularly surprising to find that 'supermultiplet' multi-isotope fits failed to converge to a completely convincing solution. A weighted fit (according to w = $1/(\sigma_{exp})^2$) returned unrealistic values of many parameters, without

reproducing the energy terms within quoted uncertainties. This led us to introduce some of the constraints detailed above, and to reduce the weights of levels known to be in strong interaction with unobserved Ω" = ½ states for which we have less confidence in the predicted energies. The parameters given in Table 5 are thus not a unique solution to this problem, but represent our best compromise retaining a realistic model with only the leading parameters optimized. The overall weighted root-mean-square deviation of the fit is 3, (with unweighted root-mean-square deviation 0.5 cm^{-1}), as illustrated in Figure 3, but the model should give reasonable predictions for higher-lying levels. These are given as supplementary data.

V Conclusion

We believe that this model offers the best predictions currently available for unobserved levels of different isotopic forms of NiH, although the predictions for rovibrational levels of the low Ω ($^2\Pi_{1/2}$ and $^2\Sigma^+$) states are not particularly secure, since few levels were actually observed and included in our model, and those few were for ^{58}NiH alone. For NiD, v = 0 of the $^2\Sigma^+$ state is predicted to lie ~2080 cm^{-1} above the lowest level of the $^2\Delta_{5/2}$ ground state. The level is sufficiently remote from others that it should be unambiguously assignable in resolved fluorescence, provided that an excitation (probably to a $^2\Pi_{3/2}$ state) can be found with significant transition dipole moments both to $^2\Sigma^+$ and any of the low-lying Ω =3/2 or 5/2 levels reported here. The situation is more delicate for higher vibrational levels, where our model places rovibrational levels J = 2.5 e parity for $^2\Sigma^+$ v=1 at 3363, $^2\Pi_{1/2}$ v=0 at 3555 and $^2\Delta_{3/2}$ v=2 at 3602 cm^{-1} (none of them being 'pure' states). The separations are even smaller for f parity levels, where the model returns $^2\Sigma^+$ v=1 at 3409 and $^2\Pi_{1/2}$ v=0 at 3530 cm^{-1}. Even small changes in the parameters result in shifts easily of the order of the rotational constants in NiD, so assignment is likely to be more difficult, particularly if, as with NiH, only one branch of a given transition to $^2\Pi_{1/2}$ appears strongly

in the spectrum. Figure 4 illustrates the predictions for $J = 2.5$ levels of NiD from this model, and those from the *ab initio* work of ref. [12]. The figure shows that the *ab initio* calculations actually match remarkably well ($|obs-calc| < 50$ cm^{-1}) for both components of the X $^2\Delta$ state. The differences between *ab initio* and supermultiplet model predictions are of the order of + 300 cm^{-1} for the $^2\Sigma^+$, $^2\Pi_{1/2}$ and $^2\Pi_{3/2}$ levels, but respect the same ordering of states (the supermultiplet fit places the $^2\Pi_{3/2}$ levels within 2 cm^{-1} of observation). The main difference between the two models is that the *ab initio* work included a modest increase in the $< {}^2\Sigma^+ | H_{SO} | {}^2\Pi_{1/2} >$ spin-orbit matrix elements as a function of internuclear distance, where our supermultiplet fit imposed a constant value.

Spectroscopic data at higher temperatures are required for example in the modeling of cool stellar atmospheres. On the basis of abundances generated by nucleosysnthesis, one might expect NiH to be observed in cool stars: Ni is second only to Fe in the transition metal abundances. Lambert and Mallia's work [50] in the early '70s found plausible coincidences with the 1930's reports of NiH emission [20,21], implying that NiH might become a molecular tracer in stellar spectra. But a later wave of interest in supplying reference transition data for NiH, notably O'Brien and co-workers using laser excitation cavity-enhanced spectroscopy [51-53], and in resolved fluorescence in Lyon [36,38,40] gave no confirmation, and our comparisons between more recent laboratory spectra and the extensive sunspot atlas now available at the Kitt Peak archive (ftp://nsokp.nso.edu/pub/atlas/) [54] suggest that the matches reported in ref [50] were accidental coincidences with very weak or blended features.

Representing energy levels of the strongly-interacting electronic states of NiH to experimental accuracy remains a spectroscopic challenge. A model taking analytical potential curves and radial spin-orbit functions rather than Dunham-type parameters should ultimately

provide a more compact set of parameters, and be better suited for extrapolation to the higher rotational levels expected to dominate in stellar spectra. Tools to do this exist. The program DUO from Yurchenko *et al.* [55], for example, has been used to predict hot spectra for many species [56]. Coupled-channel representations based on V(R) functions [57] have been very successful in describing spin-orbit perturbations between pairs of triplet and singlet states in heavy alkali dimers. Work on Rb_2 [58] and KRb [59] give just two illustrations of reduction of large data sets with the approaches of Bergeman and Stolyarov, including isotopically substituted species. But more information is needed on the heavily mixed $^2\Sigma^+$ and $^2\Pi_{1/2}$ states of NiD before we can implement this approach sensibly for NiH, underlining the need for further experimental work to access these states. We believe that the present analysis is sufficiently robust for NiD (and NiH) to give proper predictions as to where we should be looking for them.

Acknowledgements

We gratefully acknowledge financial support from the 'Programme National de Physique Stellaire' (PNPS 2016) CNRS/INSU, CEA and CNES, France.

Table 1. Effective band constants for v = 1 A(Ω=5/2), v = 1 of E(Ω=3/2) and v = 0 of I(Ω=3/2) identified in collisionally induced fluorescence of NiD. Values in cm^{-1}, with 1σ deviations in parenthesis, in units of last digit. Energies established with respect to the first ground state level, v=0, J=2.5 X $^2\Delta_{5/2}$. The parity components of the A Ω=5/2 v=1 level, resolved only above J=7.5, are not assigned, so the choice of sign for q_v is arbitrary. An avoided crossing around J = 10e leads to the large RMS deviation for this level.

Parameter	A (Ω=5/2) v=1	I (Ω=3/2) v =0	E (Ω=3/2) v =1
T_v	16657.09(2)	17362.58(1)	17503.54(2)
B_v	3.0682(9)	3.1518(5)	3.04265(101)
10^4 D_v	1.988(116)	1.216(39)	3.21(16)
10^7 H_v	-6.56(40)		5.35(68)
q_v	$1.17(12) \times 10^{-6}$	$-8.24(18) \times 10^{-4}$	$1.290(5) \times 10^{-2}$
q_D			$-7.45(35) \times 10^{-7}$
RMS deviation	0.041	0.008	0.046
J_{max}	13.5	11.5	13.5

Table 2: Band constants for the low-lying states of NiD determined from fit of term values to expression (1). Parameters in cm^{-1}, with 1σ deviations indicated in parenthesis in units of last digit. Note that e parity levels only were available for v=3 of $X_2\ ^2\Delta_{3/2}$.

State	v	G_v	B_v	$10^4\ D_v$	$10^3\ q_v$	$10^8\ q_D$	RMS dev.
$X_1\ ^2\Delta_{5/2}$	0	0.000	3.9913(6)	1.299(19)			0.004
	1	1390.156(52)	3.9012(8)	1.292(33)			0.004
	2	2742.422(50)	3.8110(6)	1.272(19)			0.005
	3	4057.041(51)	3.7217(7)	1.265(25)			0.003
	4	5334.214(56)	3.6326(9)	1.251(32)			0.008
	5	6574.095(56)	3.5439(14)	1.246(88)			0.002
$X_2\ ^2\Delta_{3/2}$	0	977.739(43)	3.9967(5)	1.475(20)	-0.888(16)		0.013
	1	2296.313(44)	3.9574(6)	0.879(32)	-6.049(32)		0.024
	2	3586.312(46)	3.8982(11)	-1.593(79)	-8.25(61)		0.177
	3	4841.961(57)	3.8139(20)	3.621(170)	-		0.120
$W_1\ ^2\Pi_{3/2}$	0	2806.840(44)	3.8553(6)	1.346(29)	-15.0(57)	-4.4(21)	0.013
	1	4175.053(46)	3.7556(10)	1.532(65)	-15.5(33)		0.019

Table 3

	$^2\Delta_{5/2}$	$^2\Delta_{3/2}$	$^2\Pi_{3/2}$	$^2\Pi_{1/2}$	$^2\Sigma^+_{1/2}$
$^2\Delta_{5/2}$	$A + 0.5\gamma + \gamma_D$ $+B(z-2) - Dz(z-3)$ $\pm 0.25q_D(z-1)(z-4)(J+0.5)$	$-\sqrt{(z-4)}\begin{bmatrix}(B-0.5\gamma)\\ -0.5\gamma_D(z+1) - 2Dz\\ \mp 0.25(z-1)(J+0.5)\times\\ (2q+p_D-q_D(z+2))\end{bmatrix}$	$\frac{-2\,B_{\nu_\Delta,\nu_\Pi}\times}{\sqrt{(J+2.5)(J-1.5)}}$	0	0
$^2\Delta_{3/2}$	*symmetric*	$-A - 1.5\gamma - \gamma_D(2z+1)$ $+B(z+2) - Dz(z+5)$ $\mp 0.5(z-1)(J+0.5)\times$ $[p+4q+p_D(z+2)-0.5q_D(5z+4)]$	$-603 f_{\nu_\Delta,\nu_\Pi} + 2\mathrm{B}_{\nu_\Delta,\nu_\Pi}$	$\frac{-2\,B_{\nu_\Delta,\nu_\Pi}\times}{\sqrt{(J-0.5)(J+1.5)}}$	0
$^2\Pi_{3/2}$	*symmetric*	*symmetric*	$0.5A + y\begin{bmatrix}B-D(y+1)\\ -0.5\gamma_D \mp 0.5q_D(J+0.5)\end{bmatrix}$	$\sqrt{y}\begin{bmatrix}-B+2D(y+1)\\ +0.5(\gamma+\gamma_D(y+2))\\ \pm 0.5(J+0.5)(0.5p_D+q+q_D(y+2))\end{bmatrix}$	$\frac{-2.1066\,B_{\nu_\Pi,\nu_\Sigma}\times}{\sqrt{(J-0.5)(J+1.5)}}$
$^2\Pi_{1/2}$	*symmetric*	*symmetric*	*symmetric*	$-0.5A + B(y+2) - \gamma$ $-D(y+1)(y+4)$ $-0.5\gamma_D(3y+4) \mp 0.5(J+0.5)\times$ $[p+p_D(y+2)+2q+q_D(3y+4)]$	$-635 f_{\nu_\Pi,\nu_\Sigma} +$ $2.1066\,B_{\nu_\Pi,\nu_\Sigma}[1 \mp (J+0.5)]$
	symmetric	*symmetric*	*symmetric*	*symmetric*	$Bx - Dx^2 + \Delta E^{(b)}_{Spin-Rotation}$

Caption to Table 3. Matrix elements of the $\mathbf{N^2}$ Hamiltonian for the $^2\Delta$, $^2\Pi$ and $^2\Sigma^+$ states and $\mathbf{R^2}$ Hamiltonian for the $^2\Delta \sim ^2\Pi \sim ^2\Sigma^+$ interactions. The upper and lower signs refer to *e* and *f* parities, respectively. [(a)] This block repeats for v = 0-5, with off-diagonal elements assumed to be zero for interactions with $\Delta v > 2$.

Footnote to table 3.

[(a)] $z = (J + 0.5)^2$, $y = z - 1$ and $x = N(N + 1)$.

[(b)] $\Delta E^{e}_{Spin-rotation} = 0.5\left(\gamma + \gamma_D x\right)\left(N\right)$ and $\Delta E^{f}_{Spin-rotation} = 0.5\left(\gamma + \gamma_D x\right)\left(N+1\right)$

Table 4. The range of observed vibrational levels, and associated ranges of term
^{x}NiH and ^{58}NiD. The complete list of term energies is available as supplementary

State	Obs (range)	^{58}NiH	^{60}NiH	^{62}NiH
	v	0-4	0-4	0-1
X $^2\Delta_{5/2}$	T_{vJ}	0-7740	0-7740	0-4170
	v	0-2	0-1	0-1
X $^2\Delta_{3/2}$	T_{vJ}	973-5730	973-5325	972-5125
	v	0-2	0-2	0
W $^2\Pi_{3/2}$	T_{vJ}	2610-6525	2610-6522	2609-4713
	v	0-1		
W $^2\Pi_{1/2}$	T_{vJ}	3454-5680[(a)]		
	v	0-1	0-1	
V $^2\Sigma^+$	T_{vJ}	2052-4095	2072-4452	

[(a)] e parity data only for $v = 1$

Table 5
Parameters (in cm^{-1}) describing the basis states $^2\Delta$, $^2\Pi$ and $^2\Sigma^+$ for ^{58}NiH from multi-isotope fit, with scaled parameters for ^{58}NiD. 1σ parameter uncertainties are quoted in units of last digit. Tables for isotopically substituted species ^{x}NiH are given as supplementary material.

State	$^2\Delta$		$^2\Pi$		$^2\Sigma^+$	
Parameter	NiH	NiD	NiH	NiD	NiH	NiD
T_e	0.0 (fixed)	0.0	2289.568(40)	2267.470	1961.242(15)	1937.179
Y_{10}	1995.651(20)	1423.6797	1892.674(32)	1350.2169	1857.622(13)	1325.2111
Y_{20}	-37.4828(52)	-19.07601	-37.5 (fixed)	-19.085	-37.5 (fixed)	-19.085
Y_{30}	0.09154 (84)	0.033235				
Y_{01}	8.0253 (13)	4.08429	7.48796 (40)	3.810824	7.6052(16)	3.87049
Y_{11}	-0.21659(78)	-0.078636	-0.22442 (15)	-0.0814788	-0.23931(74)	-0.086885
$10^3 Y_{21}$	-8.30 (11)	-2.150				
$10^4 Y_{02}$	-4.7723(100)	-1.2878(26)	-5.229 (47)	-1.3543	-4.70 (fixed)	-1.217
$10^6 Y_{12}$	5.14(40)	0.9497				
A_e	-603(fixed)	-603	-603 (fixed)	-603		
A_1	7.033(17)	5.0173				
γ_e	0.950(13)	0.4835	1.242(41)	0.63209	-0.487(21)	-0.24785
γ_1	-0.6368(57)	-0.23120				
$10^3 \gamma_D$	0.149(79)	0.03859	0.54(28)	0.140	4.50(13)	1.166
p_e	-0.00081(3)	-0.000107	-0.443(22)	-0.2255		
$10^3 p_1$	1.913(28)	0.17989				
$10^3 p_D$	-0.00362(14)	-0.0002428	3.26 (11)	0.8444		
$10^3 q_e$	0.0143(14)	0.0009593	-23.4(13)	-6.061		
$10^4 q_D$			-1.499(75)	-0.19759		
δ_{00}^H	0 (fixed)		-45 (fixed)		-49(fixed)	
$10^5 \delta_{02}^H$	-4.07 (14)					

Table 6a Vibrational overlap integrals $f_{v\Delta,v\Pi}$ and $f_{v\Pi,v\Sigma}$ (see table 3) multiplying spin-orbit parameters for ^{58}NiH and ^{58}NiD. Most were constrained to 'Initial' values (see text). 1σ parameter uncertainties are quoted in units of last digit for those optimized in the fitting procedure. Tables for isotopically substituted species are given as supplementary material.

Parameter	$^2\Delta \sim {}^2\Pi$				$^2\Pi \sim {}^2\Sigma^+$			
	NiH		NiD		NiH		NiD	
	Intial	Optimized	Initial	Optimized	Initial	Optimized	Initial	Optimized
$f_{0,0}$	0.956	0.96298(9)	0.940	0.95059(12)	0.997		0.996	
$f_{0,1}$	0.274		0.318		-0.069		-0.082	
$f_{0,2}$	0.0		0.114		0.0		-0.017	
$f_{1,0}$	-0.293	-0.29468(5)	-0.253	-0.30785 (9)	0.067		0.080	
$f_{1,1}$	0.869	0.89369 (8)	0.920	0.85476(8)	0.993		0.990	
$f_{1,2}$	0.359		0.409		-0.095		-0.115	
$f_{1,3}$	0.0		0.181		0.0		-0.031	
$f_{2,0}$	0.0		0.044		0.0		0.026	
$f_{2,1}$	-0.409	-0.41153(5)	-0.465	-0.42880(9)	0.089		0.107	
$f_{2,2}$	0.783	0.81576(8)	0.710	0.75362(26)	0.988		0.983	
$f_{2,3}$	0.405		0.451		-0.113		-0.138	
$f_{2,4}$	0.0		0.233		0.0		-0.044	
$f_{3,1}$	0.0		0.076		0.0		0.043	
$f_{3,2}$	-0.496		-0.552	-0.5376(27)	0.101		0.125	
$f_{3,3}$	0.699		0.602		0.984		0.977	
$f_{3,4}$	0.427		0.466		-0.124		-0.156	
$f_{3,5}$	0.051		0.108		0.0		0.058	
$f_{4,2}$	-0.565		-0.616		0.107		0.136	
$f_{4,3}$	0.615		0.498		0.980		0.971	
$f_{4,4}$	0.0		0.462		0.0		-0.170	
$f_{4,5}$	0.0		0.273		0.0		-0.058	
$f_{5,3}$	0.0		0.140		0.0		0.073	
$f_{5,4}$	0.0		-0.666		0.0		0.142	
$f_{5,5}$	0.0		0.400		0.0		0.966	

Table 6b. Optimized and constrained off-diagonal rotational parameters $B_{v\Delta,v\Pi}$ and $B_{v\Pi,v\Sigma}$ (in cm^{-1}) for ^{58}NiH and ^{58}NiD. Most were constrained to 'Initial' values (see text). 1σ parameter uncertainties are quoted in units of last digit for those optimized in the fitting procedure. Tables for isotopically substituted species are given as supplementary material.

	$^2\Delta \sim {}^2\Pi$				$^2\Pi \sim {}^2\Sigma^+$			
Parameter	NiH		NiD		NiH		NiD	
	Intial	Optimized	Initial	Optimized	Initial	Optimized	Initial	Optimized
$B_{0,0}$	7.292	7.653(31)	3.666	3.525(35)	7.392	7.3383(27)	3.777	
$B_{0,1}$	2.938		1.602		0.408		0.088	
$B_{0,2}$	0.0		0.683		0.0		-0.030	
$B_{1,0}$	-1.278	-1.4157(34)	-1.041	-0.976(13)	1.405		0.698	
$B_{1,1}$	6.403	7.021(18)	3.173	3.338(23)	7.102	7.0726(26)	3.659	
$B_{1,2}$	3.713		2.009		0.559		0.120	
$B_{1,3}$	0.0		1.061		0.0		-0.053	
$B_{2,0}$	0.0		0.049		0.0		0.219	
$B_{2,1}$	-1.757	-1.7922(25)	-1.234	-1.344(14)	1.871		0.940	
$B_{2,2}$	5.558	6.1156(84)	2.629	2.949(18)	6.812		3.541	
$B_{2,3}$	4.032		2.164		0.664		0.144	
$B_{2,4}$	0.0		1.336		0.0		-0.075	
$B_{3,1}$	0.0		0.084		0.0		0.360	
$B_{3,2}$	-2.088		-1.441	-1.7309(49)	2.150		1.095	
$B_{3,3}$	4.758		2.163		6.525		3.425	
$B_{3,4}$	4.094		2.178		0.746		0.163	
$B_{3,5}$	0.0		1.526		0.0		-0.097	
$B_{4,2}$	0.0		0.118		0.0		0.483	
$B_{4,3}$	-2.334		-1.584		2.321		1.200	
$B_{4,4}$	4.004		1.731		6.240		3.310	
$B_{4,5}$	0.0		2.101		0.0		0.179	
$B_{5,3}$	0.0		0.152		0.0		0.591	
$B_{5,4}$	0.0		-1.681		0.0		1.269	
$B_{5,5}$	0.0		1.334		0.0		3.195	

Table 7. Predicted energy terms (cm^{-1}) for the lowest rotational levels of NiD ar
$^2\Pi$ and $^2\Sigma^+$ 'supermultiplet' states) E < 8000 cm^{-1}). A more extensive list is given a
material. The $^2\Lambda$ labels indicate only the dominant contribution to the wavefuncti
splittings indicate severe mixing between states.

NiD					NiH		
J	E_{calc}, e parity	E_{calc}, f parity	v	State Label	J	E_{calc}, e parity	E_{calc}, f parity
0.5	2072.72	2092.62	0	$^2\Sigma^+$	0.5	2052.53	2091.15
0.5	3350.78	3366.27	1	$^2\Sigma^+$	0.5	3477.04	3454.22
0.5	3515.49	3507.16	0	$^2\Pi_{1/2}$	0.5	3851.61	3888.02
0.5	4601.43	4616.65	2	$^2\Sigma^+$	0.5	5275.97	5255.37
0.5	4825.18	4816.94	1	$^2\Pi_{1/2}$	0.5	5577.18	5610.88
0.5	5817.60	5832.78	3	$^2\Sigma^+$	0.5	6996.64	6979.43
0.5	6092.93	6084.58	2	$^2\Pi_{1/2}$	0.5	7231.05	7260.77
0.5	6998.26	7013.30	4	$^2\Sigma^+$			
0.5	7320.47	7312.05	3	$^2\Pi_{1/2}$			
0.5	8145.10	8159.63	5	$^2\Sigma^+$			
1.5	973.78	973.78	0	$^2\Pi_{3/2}$	1.5	2055.23	2132.27
1.5	2074.03	2113.78	0	$^2\Sigma^+$	1.5	2609.71	2609.83
1.5	2292.32	2292.35	1	$^2\Delta_{3/2}$	1.5	2998.95	2998.99
1.5	2802.68	2802.69	0	$^2\Pi_{3/2}$	1.5	3511.01	3465.42
1.5	3353.63	3384.45	1	$^2\Sigma^+$	1.5	3854.88	3927.47
1.5	3531.46	3514.89	0	$^2\Pi_{1/2}$	1.5	4371.23	4371.37
1.5	3582.23	3582.29	2	$^2\Delta_{3/2}$	1.5	4898.28	4898.33
1.5	4170.70	4170.71	1	$^2\Pi_{3/2}$	1.5	5308.03	5266.97
1.5	4604.27	4634.63	2	$^2\Sigma^+$	1.5	5581.36	5648.46
1.5	4837.92	4839.62	3	$^2\Delta_{3/2}$	1.5	6077.53	6077.66
1.5	4842.00	4823.92	1	$^2\Pi_{1/2}$	1.5	6715.96	6716.01
1.5	5510.71	5510.72	2	$^2\Pi_{3/2}$	1.5	7025.93	6991.83
1.5	5820.27	5850.56	3	$^2\Sigma^+$	1.5	7237.02	7295.97
1.5	6049.73	6049.70	4	$^2\Delta_{3/2}$	1.5	7708.24	7708.38
1.5	6108.30	6091.69	2	$^2\Pi_{1/2}$	1.5	8461.20	8461.25
1.5	6796.55	6796.57	3	$^2\Pi_{3/2}$			
1.5	7000.84	7030.83	4	$^2\Sigma^+$			
1.5	7264.20	7264.19	4	$^2\Pi_{3/2}$			
1.5	7335.54	7318.74	3	$^2\Pi_{1/2}$			
1.5	8052.26	8052.31	5	$^2\Delta_{3/2}$			
2.5	0.00	0.00	0	$^2\Delta_{5/2}$	2.5	0.00	0.00
2.5	993.74	993.76	0	$^2\Delta_{3/2}$	2.5	1011.68	1011.83
2.5	1389.92	1389.92	1	$^2\Delta_{5/2}$	2.5	1925.96	1925.96
2.5	2082.87	2142.37	0	$^2\Sigma^+$	2.5	2072.72	2187.79
2.5	2312.03	2312.17	1	$^2\Delta_{3/2}$	2.5	2648.44	2648.95
2.5	2741.98	2741.98	2	$^2\Delta_{5/2}$	2.5	3036.16	3036.32
2.5	2821.93	2821.97	0	$^2\Pi_{3/2}$	2.5	3559.96	3491.71

2.5	3363.62	3409.45	1	$^2\Sigma^+$	2.5	3777.75	3777.75	2	$^2\Delta_{5/2}$
2.5	3555.24	3530.62	0	$^2\Pi_{1/2}$	2.5	3872.60	3980.92	1	$^2\Sigma^+$
2.5	3601.68	3601.92	2	$^2\Delta_{3/2}$	2.5	4408.96	4409.50	1	$^2\Pi_{3/2}$
2.5	4056.37	4056.37	3	$^2\Delta_{5/2}$	2.5	4933.92	4934.10	2	$^2\Delta_{3/2}$
2.5	4189.47	4189.50	1	$^2\Pi_{3/2}$	2.5	5354.47	5293.21	1	$^2\Pi_{1/2}$
2.5	4614.15	4659.46	2	$^2\Sigma^+$	2.5	5555.92	5555.92	3	$^2\Delta_{5/2}$
2.5	4857.06	4859.39	3	$^2\Delta_{3/2}$	2.5	5599.79	5699.67	2	$^2\Sigma^+$
2.5	4865.13	4838.44	1	$^2\Pi_{1/2}$	2.5	6114.21	6114.74	2	$^2\Pi_{3/2}$
2.5	5333.31	5333.31	4	$^2\Delta_{5/2}$	2.5	6749.94	6750.11	3	$^2\Delta_{3/2}$
2.5	5528.97	5529.01	2	$^2\Pi_{3/2}$	2.5	7068.68	7018.38	2	$^2\Pi_{1/2}$
2.5	5829.83	5875.07	3	$^2\Sigma^+$	2.5	7257.17	7344.46	3	$^2\Sigma^+$
2.5	6068.34	6068.20	4	$^2\Delta_{3/2}$	2.5	7261.12	7260.97	4	$^2\Delta_{5/2}$
2.5	6131.09	6106.45	2	$^2\Pi_{1/2}$	2.5	7743.89	7744.44	3	$^2\Pi_{3/2}$
2.5	6572.99	6572.99	5	$^2\Delta_{5/2}$	2.5	8493.19	8493.38	4	$^2\Delta_{3/2}$
2.5	6814.34	6814.40	3	$^2\Pi_{3/2}$	2.5	8894.05	8894.05	5	$^2\Delta_{5/2}$
2.5	7010.19	7055.00	4	$^2\Sigma^+$					
2.5	7282.43	7282.42	4	$^2\Pi_{3/2}$					
2.5	7357.82	7332.77	3	$^2\Pi_{1/2}$					
2.5	8069.38	8069.59	5	$^2\Delta_{3/2}$					
3.5	27.93	27.93	0	$^2\Delta_{5/2}$	3.5	53.83	53.83	0	$^2\Delta_{5/2}$
3.5	1021.68	1021.73	0	$^2\Delta_{3/2}$	3.5	1065.95	1066.33	0	$^2\Delta_{3/2}$
3.5	1417.22	1417.22	1	$^2\Delta_{5/2}$	3.5	1978.01	1978.01	1	$^2\Delta_{5/2}$
3.5	2099.26	2178.35	0	$^2\Sigma^+$	3.5	2105.07	2257.57	0	$^2\Sigma^+$
3.5	2339.58	2339.94	1	$^2\Delta_{3/2}$	3.5	2702.52	2703.79	0	$^2\Pi_{3/2}$
3.5	2768.65	2768.65	2	$^2\Delta_{5/2}$	3.5	3088.17	3088.57	1	$^2\Delta_{3/2}$
3.5	2848.87	2848.96	0	$^2\Pi_{3/2}$	3.5	3623.82	3533.07	0	$^2\Pi_{1/2}$
3.5	3380.82	3441.18	1	$^2\Sigma^+$	3.5	3828.01	3828.02	2	$^2\Delta_{5/2}$
3.5	3586.79	3554.39	0	$^2\Pi_{1/2}$	3.5	3904.90	4048.24	1	$^2\Sigma^+$
3.5	3628.85	3629.44	2	$^2\Delta_{3/2}$	3.5	4461.64	4462.96	1	$^2\Pi_{3/2}$
3.5	4082.42	4082.42	3	$^2\Delta_{5/2}$	3.5	4983.72	4984.15	2	$^2\Delta_{3/2}$
3.5	4215.71	4215.80	1	$^2\Pi_{3/2}$	3.5	5415.12	5334.11	1	$^2\Pi_{1/2}$
3.5	4631.11	4691.09	2	$^2\Sigma^+$	3.5	5604.38	5604.43	3	$^2\Delta_{5/2}$
3.5	4883.71	4887.02	3	$^2\Delta_{3/2}$	3.5	5632.70	5764.37	2	$^2\Sigma^+$
3.5	4895.93	4860.52	1	$^2\Pi_{1/2}$	3.5	6165.41	6166.74	2	$^2\Pi_{3/2}$
3.5	5358.73	5358.73	4	$^2\Delta_{5/2}$	3.5	6797.39	6797.83	3	$^2\Delta_{3/2}$
3.5	5554.51	5554.60	2	$^2\Pi_{3/2}$	3.5	7124.48	7059.15	2	$^2\Pi_{1/2}$
3.5	5846.32	5906.28	3	$^2\Sigma^+$	3.5	7292.21	7406.07	3	$^2\Sigma^+$
3.5	6094.37	6093.95	4	$^2\Delta_{3/2}$	3.5	7307.83	7307.66	4	$^2\Delta_{5/2}$
3.5	6161.27	6128.95	2	$^2\Pi_{1/2}$	3.5	7793.65	7795.01	3	$^2\Pi_{3/2}$
3.5	6597.78	6597.78	5	$^2\Delta_{5/2}$	3.5	8746.09	8707.99	3	$^2\Pi_{1/2}$
3.5	6839.19	6839.37	3	$^2\Pi_{3/2}$	3.5	8893.62	8977.77	4	$^2\Sigma^+$
3.5	7026.36	7085.78	4	$^2\Sigma^+$	3.5	8939.69	8939.69	5	$^2\Delta_{5/2}$
3.5	7307.93	7307.86	4	$^2\Pi_{3/2}$					
3.5	7387.28	7354.18	3	$^2\Pi_{1/2}$					
3.5	8093.23	8093.78	5	$^2\Delta_{3/2}$					
4.5	63.82	63.82	0	$^2\Delta_{5/2}$	4.5	122.96	122.96	0	$^2\Delta_{5/2}$
4.5	1057.57	1057.67	0	$^2\Delta_{3/2}$	4.5	1135.59	1136.36	0	$^2\Delta_{3/2}$
4.5	1452.30	1452.30	1	$^2\Delta_{5/2}$	4.5	2044.85	2044.86	1	$^2\Delta_{5/2}$
4.5	2123.21	2221.69	0	$^2\Sigma^+$	4.5	2152.31	2341.47	0	$^2\Sigma^+$

4.5	2374.96	2375.68	1	$^2\Delta_{3/2}$	4.5	2771.86	2774.39	0	$^2\Pi_{3/2}$
4.5	2802.91	2802.91	2	$^2\Delta_{5/2}$	4.5	3154.89	3155.70	1	$^2\Delta_{3/2}$
4.5	2883.47	2883.66	0	$^2\Pi_{3/2}$	4.5	3702.51	3589.50	0	$^2\Pi_{1/2}$
4.5	3405.26	3479.55	1	$^2\Sigma^+$	4.5	3892.55	3892.59	2	$^2\Delta_{5/2}$
4.5	3626.07	3586.22	0	$^2\Pi_{1/2}$	4.5	3951.87	4129.28	1	$^2\Sigma^+$
4.5	3663.72	3664.89	2	$^2\Delta_{3/2}$	4.5	4529.16	4531.79	1	$^2\Pi_{3/2}$
4.5	4115.88	4115.88	3	$^2\Delta_{5/2}$	4.5	5047.59	5048.45	2	$^2\Delta_{3/2}$
4.5	4249.43	4249.59	1	$^2\Pi_{3/2}$	4.5	5489.75	5389.68	1	$^2\Pi_{1/2}$
4.5	4655.16	4729.47	2	$^2\Sigma^+$	4.5	5666.44	5666.73	3	$^2\Delta_{5/2}$
4.5	4917.91	4922.52	3	$^2\Delta_{3/2}$	4.5	5680.49	5842.41	2	$^2\Sigma^+$
4.5	4934.29	4890.14	1	$^2\Pi_{1/2}$	4.5	6231.03	6233.66	2	$^2\Pi_{3/2}$
4.5	5391.39	5391.39	4	$^2\Delta_{5/2}$	4.5	6858.21	6859.11	3	$^2\Delta_{3/2}$
4.5	5587.31	5587.49	2	$^2\Pi_{3/2}$	4.5	7192.77	7114.16	2	$^2\Pi_{1/2}$
4.5	5869.77	5944.15	3	$^2\Sigma^+$	4.5	7342.51	7480.63	3	$^2\Sigma^+$
4.5	6127.79	6126.77	4	$^2\Delta_{3/2}$	4.5	7367.90	7367.60	4	$^2\Delta_{5/2}$
4.5	6198.82	6159.39	2	$^2\Pi_{1/2}$	4.5	7857.40	7860.10	3	$^2\Pi_{3/2}$
4.5	6629.65	6629.65	5	$^2\Delta_{5/2}$	4.5	8595.00	8596.01	4	$^2\Delta_{3/2}$
4.5	6871.10	6871.45	3	$^2\Pi_{3/2}$	4.5	8806.22	9049.31	4	$^2\Sigma^+$
4.5	7049.37	7123.12	4	$^2\Sigma^+$	4.5	8949.86	8763.48	3	$^2\Pi_{1/2}$
4.5	7340.66	7340.43	4	$^2\Pi_{3/2}$	4.5	8998.31	8998.31	5	$^2\Delta_{5/2}$
4.5	7423.91	7383.06	3	$^2\Pi_{1/2}$					
4.5	8123.73	8124.90	5	$^2\Delta_{3/2}$					

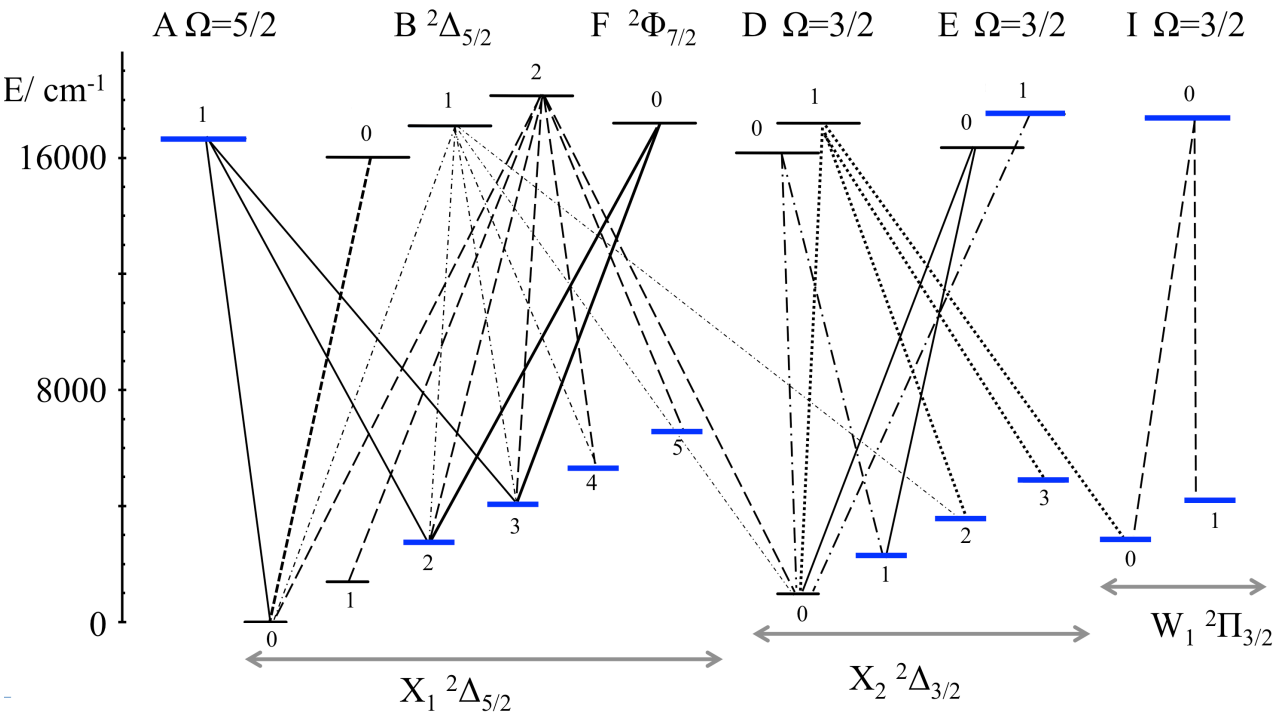

FIG. 1. (colour online) Emission bands observed in laser-induced fluoresence spectra of NiD. Thicker (blue) lines indicate hitherto unobserved vibrational levels in these electronic states.

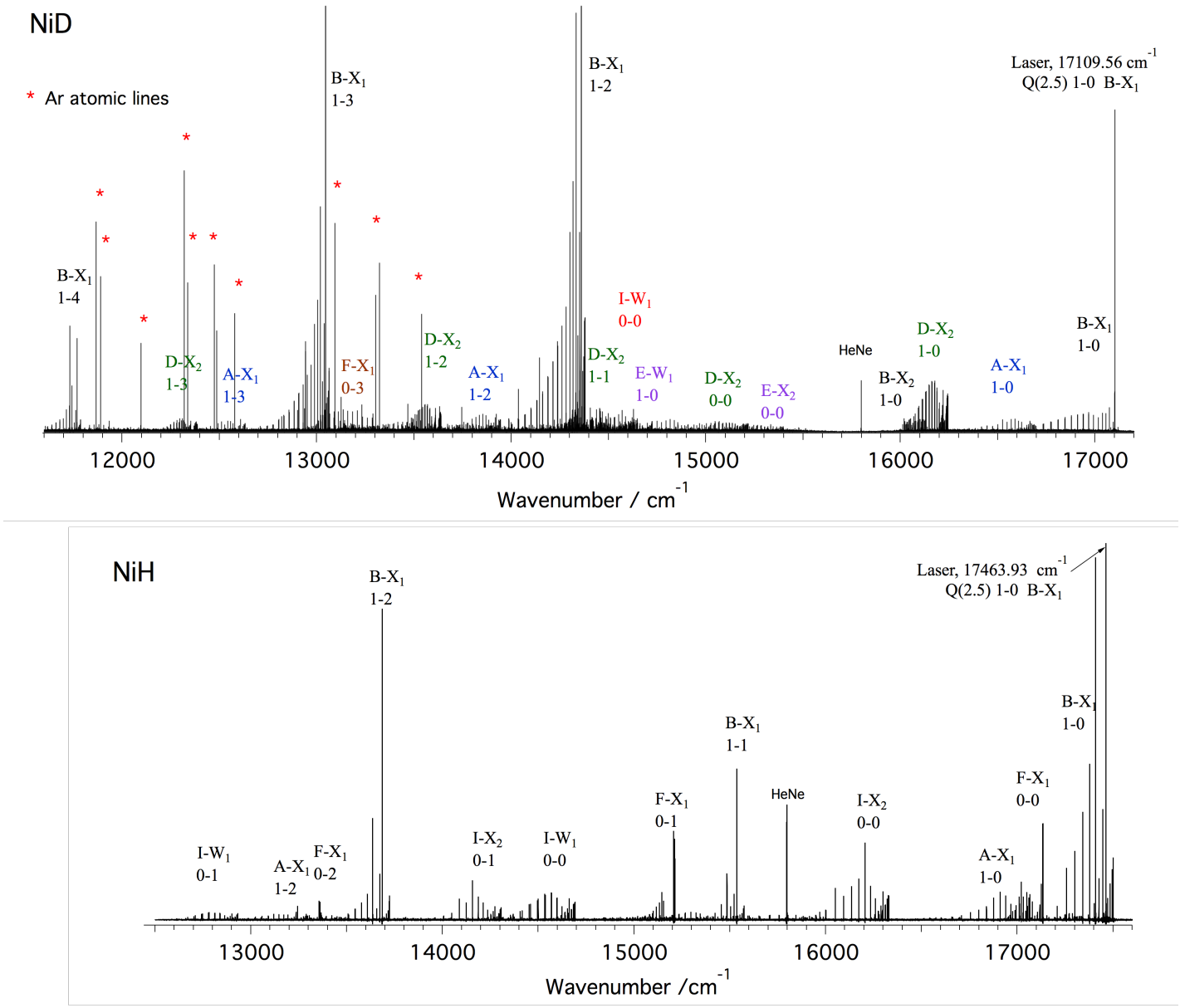

Figure 2. (colour online) Resolved fluorescence spectra of NiD and NiH (resolution 0.04 cm^{-1}) showing collisionally-induced transitions from several electronic systems. In both cases, the laser excited $Q_{ef,fe}$ (2.5) $B–X_1$ (1-0). Some lines (notably around 14800 cm^{-1}) remain unassigned in the NiD spectrum. The Ar lines (*) are also present in the NiH spectrum, but are much weaker than the molecular emission.

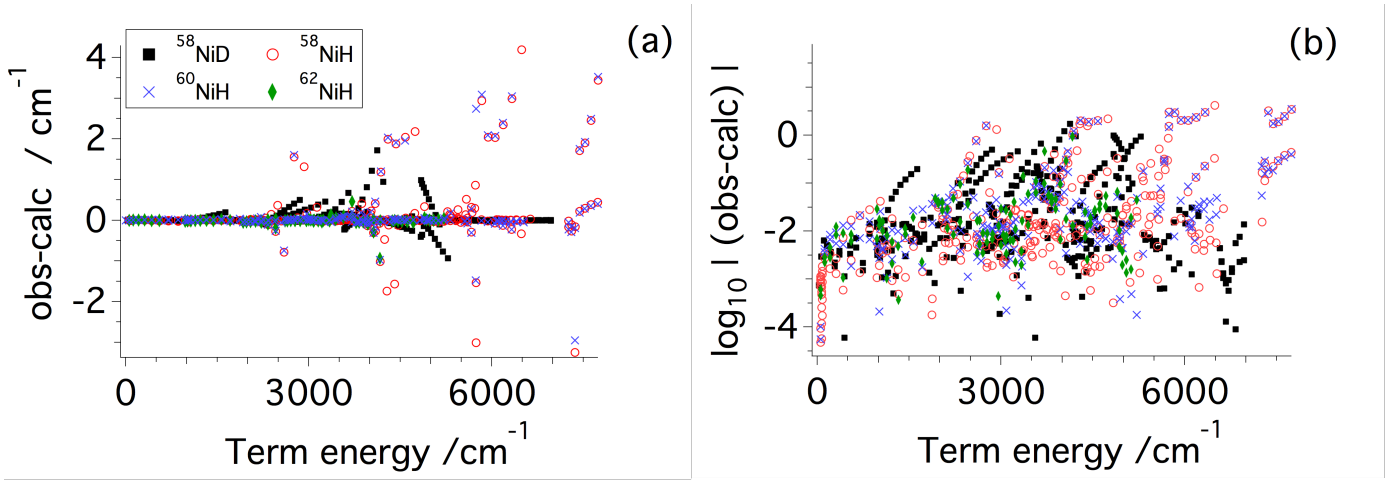

Figure 3. (colour online) Distribution of obs-calc residuals generated from the multi-isotope fit. The logarithmic scale in panel (b) illustrates more clearly the distribution of residuals < 0.05 cm^{-1}, indistinguishable in panel (a).

Figure 4. (colour online) Comparison between predicted term values for ^{58}NiD at $J = 2.5$ from our multi-isotope fit (thick lines), and from *ab initio* calculations of C. Marian [12], (thinner (blue) lines). Labels indicate the dominant wavefunction contribution $^2\Lambda_\Omega$ and vibrational levels. Connectors (red) link predictions for the $\Omega = ½$ states. Asterisks indicate experimentally observed levels.

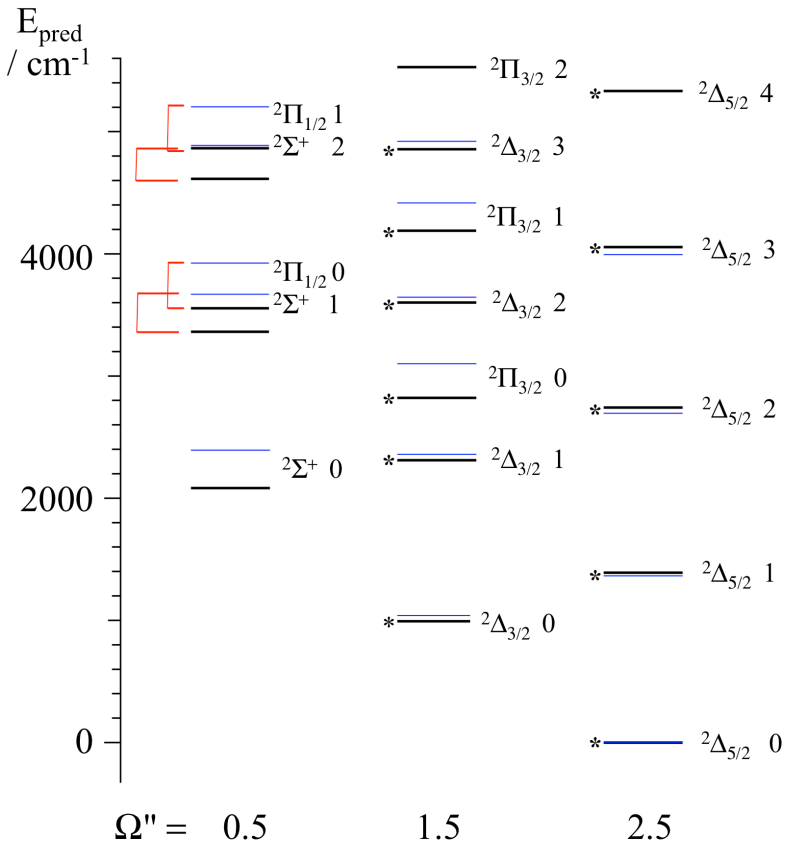

References

[1] S.R. Langhoff and C.W. Bauschlicher, *Ann. Rev. Phys. Chem.* **39**, 181 (1988).

[2] M.R.A. Blomberg, P.E.M. Seigbahn, and B.O. Roos, *Mol. Phys.* **47**, 127 (1982).

[3] B.I. Dunlap and H.L. Yu, *Chem. Phys. Lett.* **73** (3), 525 (1980).

[4] M.P. Guse, R.J. Blint, and A.B. Kunz, *International Journal of Quantum Chemistry* **11** (5), 725 (1977).

[5] N.J. Mayhall and K. Raghavachari, *J. Chem. Theo. & Comp.* **6** (9), 2714 (2010).

[6] P.S. Bagus and C. Bjorkman, *Phys. Rev. A* **23** (2), 461 (1981).

[7] S.P. Walch and C.W. Bauschlicher, *Chem. Phys. Lett.* **86** (1), 66 (1982).

[8] S.P. Walch and C.W. Bauschlicher, *J. Chem. Phys.* **78** (7), 4597 (1983).

[9] F. Ruette, G. Blyholder, and J. Head, *J. Chem. Phys.* **80** (5), 2042 (1984).

[10] R. Pouamerigo, M. Merchan, I. Nebotgil, P.A. Malmqvist, and B.O. Roos, *J. Chem. Phys.* **101** (6), 4893 (1994).

[11] C.M. Marian, *J. Chem. Phys.* **93** (2), 1176 (1990).

[12] C.M. Marian, *Ber. Bunsen Phys. Chem.* **99** (3), 254 (1995).

[13] W.L. Zou and W.J. Liu, *J. Comp. Chem.* **28** (14), 2286 (2007).

[14] J.H. Chen and T.C. Steimle, *Chem. Phys. Lett.* **457** (1-3), 23 (2008).

[15] S.P. Walch, C.W. Bauschlicher, and S.R. Langhoff, *J. Chem. Phys.* **83** (10), 5351 (1985).

[16] D.P. Chong, S.R. Langhoff, C.W. Bauschlicher, and S.P. Walch, *J. Chem. Phys.* **85** (5), 2850 (1986).

[17] C.W. Bauschlicher, S.R. Langhoff, and A. Komornicki, *Theoretica Chimica Acta* **77** (4), 263 (1990).

[18] C.V. Diaconu, A.E. Cho, J.D. Doll, and D.L. Freeman, *J. Chem. Phys.* **121** (20), 10026 (2004).

[19] S. Goel and A.E. Masunov, *J. Chem. Phys.* **129** (21), 214302 (2008).

[20] A.G. Gaydon and R.W.B. Pearse, *Proc. Roy. Soc. London A* **148**, 312 (1935).

[21] A. Heimer, *Z. Phys.* **105** (1), 56 (1937).

[22] N. Aslund, H. Neuhaus, Lagerqvist. A, and E. Andersen, *Arkiv for Fysik* **28** (3), 271 (1965).

[23] T.C. Devore, *High Temperature Science* **12** (4), 259 (1980).

[24] R. Scullman, S. Löfgren, and S. Adakkai Kadavathu, *Phys. Scr.* **25** (2), 295 (1982).

[25] S. Adakkai Kadavathu, S. Lofgren, and R. Scullman, *Phys. Scr.* **35** (3), 277 (1987).

[26] S. Adakkai Kadavathu, R. Scullman, R.W. Field, J.A. Gray, and M. Li, *J. Mol. Spectrosc.* **147**, 448 (1991).

[27] S. Adakkai Kadavathu, R. Scullman, J.A. Gray, M. Li, and R.W. Field, *J. Mol. Spectrosc.* **140**, 126 (1990).

[28] T. Nelis, S.P. Beaton, K.M. Evenson, and J.M. Brown, *J. Mol. Spectrosc.* **148**, 462 (1991).

[29] S.P. Beaton, K.M. Evenson, T. Nelis, and J.M. Brown, *J. Chem. Phys.* **89** (7), 4446 (1988).

[30] K. Lipus, U. Simon, E. Bachem, T. Nelis, and W. Urban, *Mol. Phys.* **67** (6), 1431 (1989).

[31] K. Lipus, E. Bachem, and W. Urban, *Mol. Phys.* **75** (4), 945 (1992).

[32] K. Lipus, W. Urban, K.M. Evenson, and J.M. Brown, *Mol. Phys.* **79** (3), 571 (1993).

[33] J.A. Gray and R.W. Field, *J. Chem. Phys.* **84** (2), 1041 (1986).

[34] C.W. Bauschlicher and B.O. Roos, *J. Chem. Phys.* **91**, 4785 (1989).

[35] M.C. McCarthy, H. Kanamori, T.C. Steimle, M.G. Li, and R.W. Field, *J. Chem. Phys.* **107** (11), 4179 (1997).

[36] H. Harker, C. Richard, G. Tourasse, P. Crozet, and A.J. Ross, *J. Mol. Spectrosc.* **292**, 28 (2013).

[37] J.A. Gray, M. Li, T. Nelis, and R.W. Field, *J. Chem. Phys.* **95**, 7164 (1991).

[38] A.J. Ross, P. Crozet, C. Richard, H. Harker, S.H. Ashworth, and D.W. Tokaryk, *Mol. Phys.* **110** (17), 2019 (2012).

[39] R. Vallon, C. Richard, P. Crozet, G. Wannous, and A. Ross, *Astrophys. J.* **696** (1), 172 (2009).

[40] R. Vallon, S.H. Ashworth, P. Crozet, R.W. Field, D. Forthomme, H. Harker, C. Richard, and A.J. Ross, *J. Phys. Chem. A* **113** (47), 13159 (2009).

[41] J.M. Brown, E.A. Colbourn, J.K.G. Watson, and F.D. Wayne, *J. Mol. Spectrosc.* **74** (2), 294 (1979).

[42] J.M. Brown, A.S.C. Cheung, and A.J. Merer, *J. Mol. Spectrosc.* **124** (2), 464 (1987).

[43] J.M. Brown and A.J. Merer, *J. Mol. Spectrosc.* **74** (3), 488 (1979).

[44] H. Lefebvre-Brion and R.W. Field, *The spectra and dynamics of diatomic molecules* (Elsevier, Amsterdam, 2004), p. 766.

[45] R.J. Le Roy, *J. Mol. Spectrosc.* **194** (2), 189 (1999).

[46] J.M. Brown and J.K.G. Watson, *J. Mol. Spectrosc.* **65** (1), 65 (1977).

[47] R.J. Le Roy, *J. Quant. Spectrosc. Rad. Trans.* **186**, 167 (2017).

[48] R.J. Le Roy, *J. Quant. Spectrosc. Rad. Trans.* **186**, 158 (2017).

[49] R.J. Le Roy, *J. Quant. Spectrosc. Rad. Transf.* **186**, 197 (2017).

[50] D.L. Lambert and E.A. Mallia, *Mon. Not. Roy. Astron. Soc.* **151** (4), 437 (1971).

[51] L.C. O'Brien and J.J. O'Brien, *Astrophys. J.* **621** (1), 554 (2005).

[52] S. Shaji, J. Nunn, J.J. O'Brien, and L.C. O'Brien, *Astrophys. J.* **672**, 722 (2008).

[53] S. Shaji, A. Song, M. Li, J.J. O'Brien, and L.C. O'Brien, *Canad. J. Phys.* **87** (5), 583 (2009).

[54] L. Wallace, K. Hinkle, and W. Livingston, *NSO technical report ; 00-01* **An atlas of sunspot umbral spectra in the visible, from 15,000 to 25,500 cm(-1) (3920 to 6664 [Angstrom])** (2000).

[55] S.N. Yurchenko, L. Lodi, J. Tennyson, and A.V. Stolyarov, *Computer Physics Communications* **202**, 262 (2016).

[56] J. Tennyson and S.N. Yurchenko, *Mon. Not. Roy. Astron. Soc.* **425** (1), 21 (2012).

[57] O. Dulieu and P.S. Julienne, *J. Chem. Phys.* **103** (1), 60 (1995).

[58] A.N. Drozdova, A.V. Stolyarov, M. Tamanis, R. Ferber, P. Crozet, and A.J. Ross, *Phys. Rev. A* **88**, 022504 (2013).

[59] K. Alps, A. Kruzins, M. Tamanis, R. Ferber, E.A. Pazyuk, and A.V. Stolyarov, *J. Chem. Phys.* **144** (14), 144310 (2016).